Radiation Physics and Chemistry 214 (2024) 111283

Contents lists available at ScienceDirect

Radiation Physics and Chemistry

journal homepage: www.elsevier.com/locate/radphyschem

Spectrometric performance of SiC radiation detectors at high temperature

M.C. Jiménez-Ramos [a,b,*], A. García Osuna [a], M. Rodriguez-Ramos [a], E. Viezzer [c], G. Pellegrini [d], P. Godignon [d], J.M. Rafí [d], G. Rius [d], J. García López [a,c]

[a] Centro Nacional de Aceleradores (U. Sevilla, CSIC, J. de Andalucia), 41092, Seville, Spain
[b] Dpto. de Física Aplicada II, Universidad de Sevilla, 41012, Seville, Spain
[c] Dpto. de Física Atómica, Molecular y Nuclear, Universidad de Sevilla, 41012, Seville, Spain
[d] Institute of Microelectronics of Barcelona, IMB-CNM-CSIC, 08193, Barcelona, Spain

ARTICLE INFO

Handling Editor: Dr. Chris Chantler

Keywords:
SiC detector
High-temperature
Nuclear fusion plasmas
Alpha particle detection
Electron-hole pair

ABSTRACT

In this work, we have investigated the performance of a 4H–SiC radiation sensor in the temperature range from 25 °C to 450 °C to explore its compatibility as detector of fast ion losses in plasma diagnostic of future nuclear fusion reactors. To simulate the escape of fusion-born alpha particles in D-T (deuterium-tritium) fusion plasmas, spectroscopic measurements were carried out in a vacuum chamber by irradiating the detector with a 3.5 MeV alpha beam from a Tandem accelerator. The detector was found to have an energy resolution ≤2% over the entire temperature range analyzed. Relevantly, the excellent spectrometric capabilities of the device have allowed us to calculate from experimental data, with unprecedented accuracy, the average energy required to create a single electron-hole pair in 4H–SiC as a function of temperature.

1. Introduction

In fusion burning plasmas, suprathermal particles called fast ions are responsible for the plasma heating, thus being the main source of energy and momentum [Thyagaraja et al., 2007]. However, several loss mechanisms can induce a degradation of the plasma efficiency and jeopardize the integrity of the device vessel due to the heat load produced by the ions escaping from the plasma [White et al., 1995]. For the design and proper operation of nuclear fusion reactors, a good understanding of the interplay between fast-ions and the losses mechanisms is essential to improve the fusion performance. Currently, the main diagnostic tool to study the physics underlying the particle-wave interaction mechanisms is the Fast Ion Loss Detector (FILD) [Rivero-Rodriguez et al., 2018]. Based on scintillator materials, provides full information on velocity-space [García-Muñoz et al., 2009; Galdon-Quiroga et al., 2018] and absolute fluxes [Rodriguez-Ramos et al., 2017] of the ions escaping from the plasma. However, in the next generation of fusion reactors like ITER (International Thermonuclear Experimental Reactor), given the complexity of the response of the scintillator under extreme radiation conditions and temperature (thermal quenching) [Rodríguez-Ramos et al., 2017], the FILD design [Garcia-Munoz et al., 2016] may not meet the specifications required to detect the 3.5 MeV alpha particles resulting from the D-T reaction. The best alternative at present is to use solid-state detectors based on a wide bandgap material, like diamond or silicon carbide (SiC) instead of silicon [Dankowski et al., 2017; Jiménez-Ramos et al., 2020]. Diamond, both natural and synthetic, presents excellent spectroscopic response at high temperatures [Crnjac et al., 2020], however, the polarization phenomena, its high price and the difficulty of manufacturing devices bigger than few mm^2 restrict its use in many real applications as a sensor [Ramos et al., 2021; 2022].

Differently, SiC is a wide bandgap (3.23 eV for 4H-polytype), highly thermally-conductive material (3.7 W/(cm·°C)) [Levinshtein et al., 2001], suitable for high temperature applications [Lebedev et al., 2021; Medina et al., 2023]. It has also been used to study nuclear physics aspects in hot plasmas [Cavallaro et al., 2014] and for detecting radiation and particles emitted by laser-generated plasmas [Torrisi and Cannavò, 2016] with excellent signal to noise ratios, fast response and nanosecond time resolution in time of flight measurements [Torrisi, 2014]. To study the spectroscopic response in semiconductors, a powerful method is the Ion Beam Induced Charge (IBIC) technique, based on charge injection using mono-energetic ion beams [Breese, 1993, Pezzarossa et al., 2021]. In IBIC, the ionizing radiation produces a certain number of free carriers along the track, which are proportional to the energy deposited by the impinging radiation in the active volume of the detector. The electrons/holes are forced to drift towards the electrodes under the influence of

* Corresponding author. Centro Nacional de Aceleradores (U. Sevilla, CSIC, J. de Andalucia), 41092, Seville, Spain.
E-mail address: mcyjr@us.es (M.C. Jiménez-Ramos).

https://doi.org/10.1016/j.radphyschem.2023.111283
Received 8 June 2023; Received in revised form 29 July 2023; Accepted 16 September 2023
Available online 22 September 2023

an electric field corresponding to the applied bias voltage. During their motion, the charge carriers induce a measurable signal in the readout electrode, which can be processed with proper electronics. The Charge Collection Efficiency (CCE) is a key parameter in the IBIC technique, defined as the ratio of the collected charge to the generated charge from the incoming radiation. In this work, we study the spectroscopic performance of a 4H–SiC PN diode (PND) for the detection of 3.5 MeV alpha particles in a wide temperature range, from room temperature (RT) and up 450 °C, which aims to mimic the real conditions of a working fusion reactor [Aumeunier et al., 2017]. In addition, the measured spectra were used to calculate the average electron-hole pair creation energy as a function of temperature with better accuracy than the previous works available in the literature [Garcia et al., 2013]. This paper is organized as follows: after an introduction given in Section 1, the description of the detector, the experimental setup and tests performed are described in Section 2. In Section 3, the main experimental results are presented and discussed. Finally, Section 4 concludes the paper with a summary of the results of this work.

2. Experimental details

The detector was manufactured at the Institute of Microelectronics of Barcelona [Instituto de Microelectrónica de Barcelona, 2023] and built on a n^+-type 4H–SiC wafer of ~350 μm thickness. Its active layer thickness is ~40 μm when the detector is biased at − 300 V, i.e. much thicker than the penetration range of 3.5 MeV alpha particles in SiC, which can be estimate in ~9.8 μm. With an active area of 3 × 3 mm^2, a low doped 500 nm thick p^+ layer was formed by Al ion implantation, which was applied before the deposition of the passivation layer (SiO_2 (100 nm) + Si_3N_4 (500 nm)). The front metal contact pad consists of a multilayer structure consisting in Au (150 nm) + Ti (150 nm). Its completed schematic layout can be found in Fig. 1. The electrical characterization of the detector was carried out on a light-proof and electrically shielded Summit 11000 B-M probe station, using a Keithley 2470 Source-Meter Unit (SMU) for the current-voltage (I–V) measurements (Fig. 2a) and an Agilent 4284 A Precision LCR-Meter to determine the capacitance-voltage (C–V) characteristics (Fig. 2b) at 10 kHz. For high temperature applications, the PND was encapsulated by the Alter Technology company [Alter Technology company, 2023] in a TO-257, which consists in a hermetic metal case, but was used with the top cover removed, while gold wire bondings were used for the electrical contacts.

During the characterization of the device, the detector was exposed to various thermal cycles. In the context of this work, a thermal cycle refers to a series of measurements during which the detector was either heated or cooled.

The study of the spectroscopic response of the detector has been done at the 3 MV Tandem Pelletron (NEC) accelerator of the National Accelerator Center (CNA, Seville) [García López et al., 2000; Gómez-Camacho et al., 2021]. The IBIC measurements were performed in a vacuum chamber (~10^{-6} mbar) specifically developed for high temperature applications. The chamber is equipped with a ceramic thermal heater with a temperature control system, which allows the heating of an electrically isolated sample holder (150 mm × 150 mm) placed in front of the heater to temperatures up to 500 °C. The temperature uniformity is monitored and controlled using two thermocouples placed at the center and the corner of the sample holder. A more detailed description of the chamber can be found in [Rodríguez Ramos, 2017]. For the IBIC experiments, a monoenergetic 3.5 MeV He^{2+} beam was employed. The ion beam passed through a collimator of 80 μm in diameter before reaching the detector, which allows to keep the counting rate to around 100 cps and to prevent creating structural damage to the device during the measurements. A scintillator material (Y_2O_3:Eu^{3+}) with excellent emission yield to light ions [Jiménez-Ramos et al., 2014] was also installed in parallel to the detector to localize the beam spot through a high-resolution CCD camera placed in one external port of the vacuum chamber. The movement of the holder is controlled by stepping motors capable to provide linear displacement in both axis with a 10 μm spatial resolution, therefore providing a fine control of the irradiation zone and positioning. To avoid additional electronic noise during the measurements; the thermal heater was switched off during the IBIC characterization, once the set temperature was reached. It is important to note that with the count rate used, an acquisition time of a few seconds for each spectrum was sufficient to obtain good statistics, so that the temperature difference of the sample holder measured before and after the irradiation was guaranteed to be kept below ±5 °C with respect to the temperature set point. A schematic of the experimental setup and the standard electronic chain for spectroscopy applications (same setup as in the previous work [Garcia Lopez et al., 2016]) is shown in Fig. 3. To get the signal out of the detector, the TO-257 pins were mechanically attached to copper wires, which extend out of the sample holder to a low temperature zone where they were connected to a coaxial cable through a two-pole BNC M screw connector. The detector was reverse biased using a Tennelec 953 High Voltage Power Supply, which also provided the value of the leakage current. Pulse height spectra were acquired using a Canberra 2003 B T preamplifier with a modified internal resistance of 10 MΩ to reduce the voltage drop across the bias resistor when the leakage current increased with the temperature [Simon and Sze, 2002]. At each temperature, the applied voltage was adjusted to compensate for this drop in voltage. A Tennelec TC 245

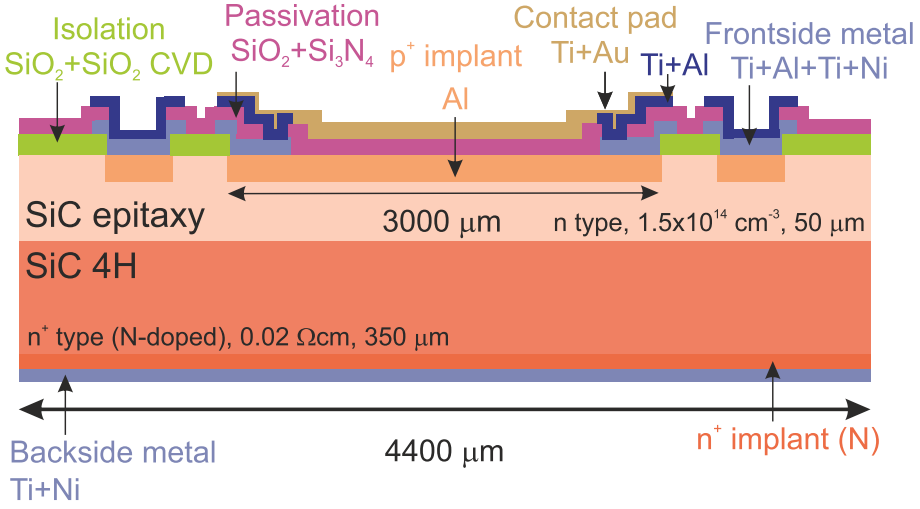

Fig. 1. Schematic cross section (not to scale) of the 4H–SiC PND employed for high-temperature measurements.

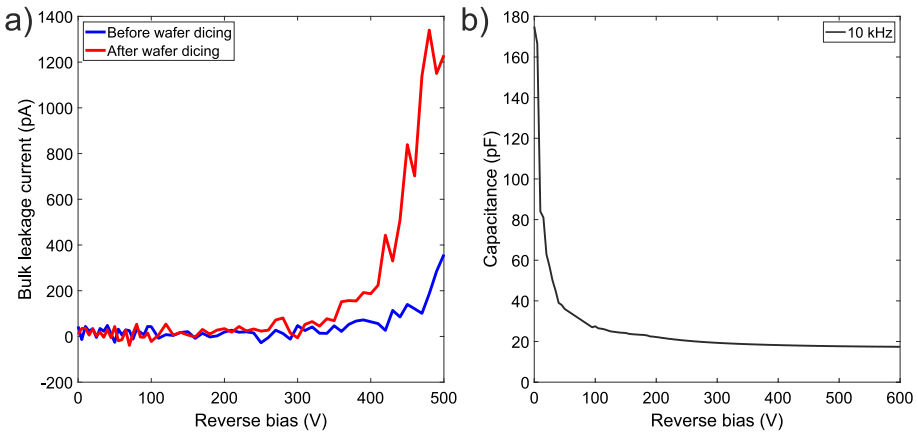

Fig. 2. A) Bulk leakage current as a function of the bias voltage before (blue) and after (red) the slicing process. b) Capacitance as a function of the bias voltage measured at 10 kHz.

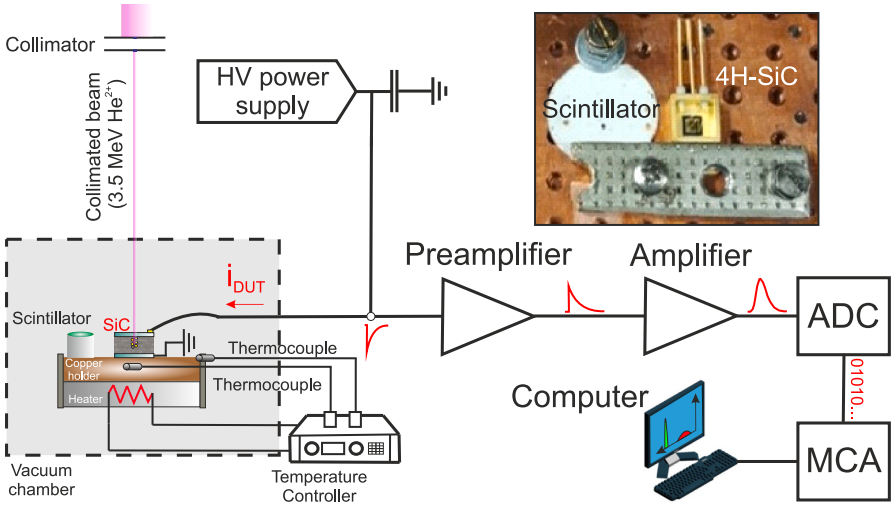

Fig. 3. Scheme of the experimental setup: The detector and a scintillator were installed in a movable holder controlled by stepping motors. An 80 μm collimator was placed in front of the holder to limit the count rate.

amplifier with the shaping time set to 1.5 μs and a Canberra ADC 8715 completed the processing electronic chain. The spectra were acquired using GENIE-2000 Basic Spectroscopy V3.1 software.

3. Results

3.1. Charge collection efficiency

Prior to the studies at high temperature, the homogeneity of the CCE across the surface of the detector was determined at RT by using the ion beam μ-probe of the CNA. To achieve this, a 3.5 MeV He^{2+} focused beam with spatial resolution ~2 μm was used to scan the full area of the detector. The resulting IBIC map is shown in Fig. 4. It was acquired by biasing the detector at − 200 V and with a counting rate of ~300 Hz. The IBIC map revealed a high level of homogeneity in the detector's CCE values across its entire active surface. The standard deviation of the CCE values was around 1.3% in the full charge collection region (100% - red area). This high level of homogeneity ensures that the results obtained in the high temperature chamber will not depend on the impact point of the beam on the detector. Note that in three corners of the detector there is a small square with an apparent CCE greater than 100%, which correspond to windows for potential electrical bondings, through which the alpha particles deposit more energy into the active volume of the device.

3.2. Multichannel analyser (MCA) calibration

As it will be shown in section 3.4, the change in detector temperature introduces a shift in the measured signals due to the change in electron-hole pair formation energy, ϵ_{4H-SiC}. In order to determine with accuracy the value of ϵ_{4H-SiC} in the investigated temperature range, a precise calibration of the MCA is necessary. The full electronic chain (preamplifier, amplifier, ADC and MCA) was calibrated at room temperature using a triple alpha source (^{239}Pu, ^{241} Am and ^{244}Cm) and the energy peak of the 3.5 MeV He^{2+} beam. To assess the correct assignment of the energy of the peaks from the spectra, the energy loss of the ions as they pass through the dead layers of the detector (i.e., the front metallization and passivation layers) has been simulated with the Montecarlo software SRIM (Ziegler et al., 2008]. The average energy loss in the dead layers was estimated to be 210 keV for the 3.5 MeV He ion beam. The pulse height spectra and the energy calibration curve are shown in Fig. 5. The detector presents a linear response in the range of the energies measured (Inset in Fig. 5).

Both this calibration and the subsequent high temperature measurements were performed with the detector biased to − 40 V. This value corresponds to the onset of the plateau of the CCE curve measured for the ^{244}Cm emission (Fig. 6a), which are the most energetic alpha particles used during calibration indicating that the depletion width is large enough to completely stop the ^{244}Cm alpha particles. In addition, at this

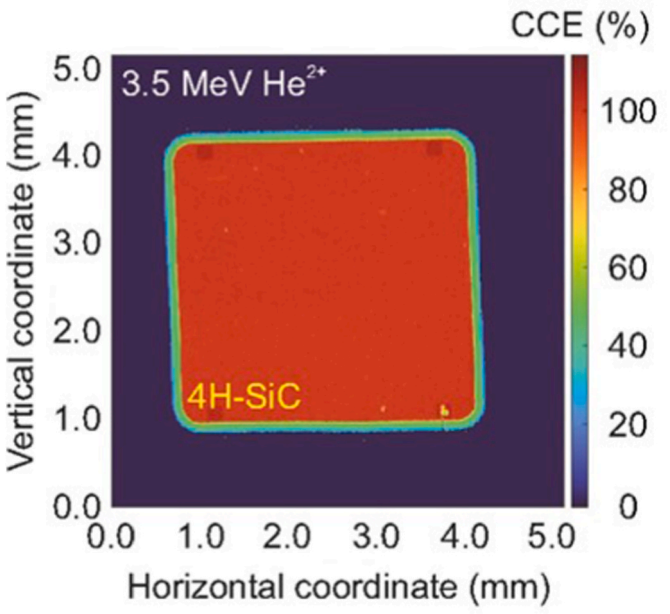

Fig. 4. IBIC map showing the average CCE of the detector biased at −200 V obtained with 3.5 MeV He^{2+} beam. The homogeneous response spans the whole detector area, where red is an indication of 100% CCE.

bias voltage, the resolution of the 3.5 MeV alpha peak has already reached the minimum value of the room temperature resolution (Fig. 6b). These are, therefore, the working conditions that guarantee a CCE of 100% while minimizing the leakage current of the detector.

3.3. Leakage current and energy resolution as a function of temperature

The leakage current values have been measured as a function of temperature for all the performed thermal cycles. Leakage current is the result of several distinct contributions: the bulk leakage current (I_B), the surface leakage current (I_S) and a 3rd term due to different components of the experimental setup (connectors, cables, absorption of moisture, …). For good quality detectors I_B is caused by thermal generation of electron-hole pairs in the depleted region and from the motion of minority carriers across the junction. For a PN junction diode, it is an increasing function of the temperature [Leroy and Rancoita, 2012]. On the other hand, I_S typically attributed to both the manufacturing processes of the complete device and an improper handling of the detectors (such as scratches, surface pollution, …). The dependence on temperature for the last two components is very difficult to predict.

Two distinctive behaviors have been found for the leakage current values of the 1st heating cycle with respect to the following cooling cycle and the rest of the series made in the range from RT up to 450 °C.

During the 1st heating cycle, a rapid increase in leakage current was observed starting at 150°C, reaching a maximum value of ~3 μA at 300–350°C, then dropping to ~1 μA at 450°C (Fig. 7). During the cooling down cycle to RT the leakage current continued to decrease, so

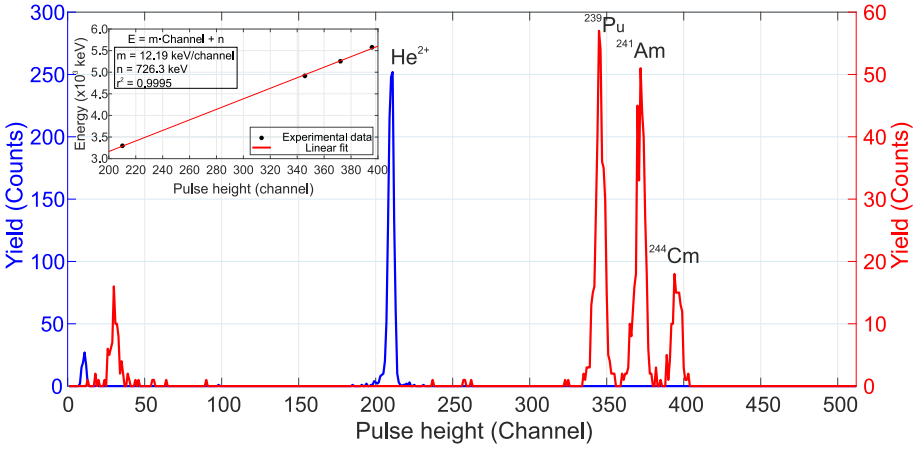

Fig. 5. Pulse height spectra for calibration and (Inset) energy calibration curve. The detector was reverse biased at −40 V.

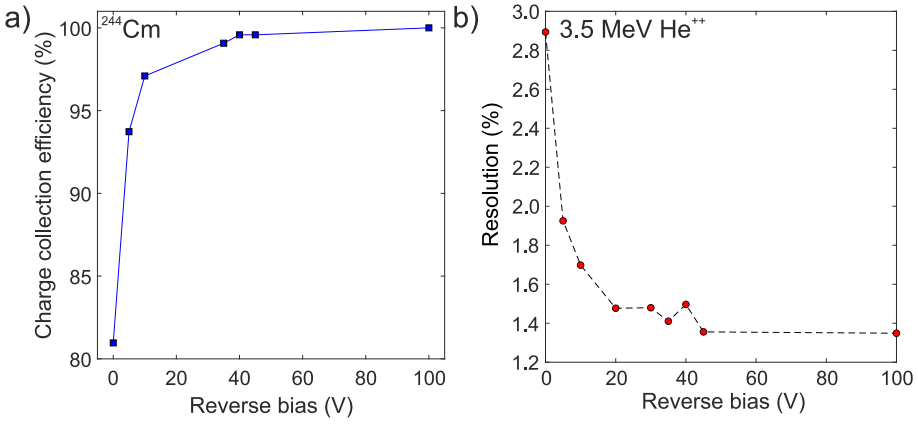

Fig. 6. A) CCE curve obtained with the highest energy emission from the triple alpha source (^{244}Cm). b) Energy resolution as a function of the bias voltage for the 3.5 MeV He beam at room temperature.

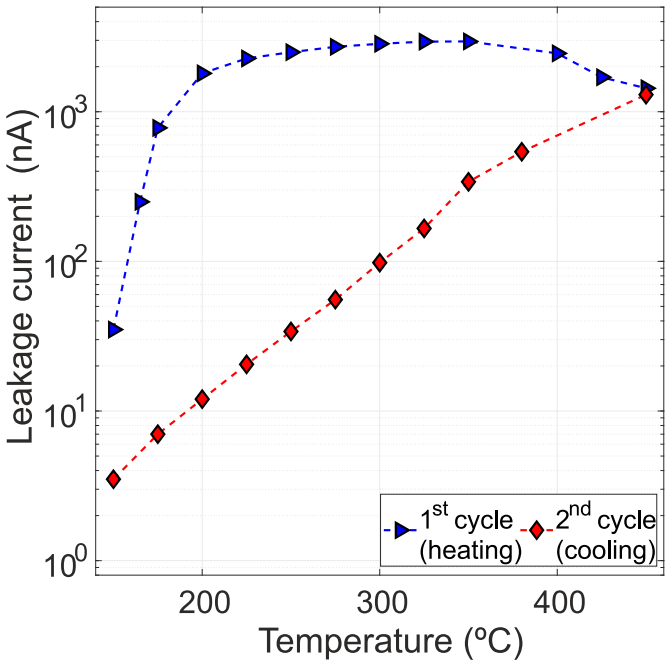

Fig. 7. Leakage current as a function of temperature for the 1st heating and subsequent cooling cycle. The current meter only measures values greater than 1 nA.

that the spectra measured during this 2nd cycle exhibit much better resolution than during the previous heating. This unintentional change is significantly beneficial to the quality of the signal in terms of the shape of the peaks and the resolution of the spectra, as shown in Fig. 8.

The spectrum corresponding to the 1st cycle presents an energy resolution R ≈ 1.5% up to 150 °C, calculated from the Full Width at Half Maximum (FWHM) of the peak divided by the location of the peak centroid. This value is comparable to the values reported in the literature for high quality SiC detectors measured at RT [Jiménez-Ramos et al., 2020, Nava et al., 2008a]. Additionally, it should be noted that the detector in this study was biased at a low voltage (− 40 V) compared to its nominal fully-depletion voltage (− 300 V). The energy resolution improves with the applied voltage [Nava et al., 2006], making this result a clear indication of the device's actual good spectrometric quality, which is shown later. However, the rapid increase in leakage current observed during the 1st heating cycle from 150 °C results in a strong broadening of the alpha peak at 200 °C and even in the appearance of a low energy tail for measurements at 300 °C, where the leakage current reached its maximum value. In the temperature range 250–350 °C, we obtained a poor energy resolution R ≈ 18%, due to the increase of the electronic noise. Fortunately, the unknown process that produced the anomalous increase in leakage current and noise disappeared as the temperature rose above 350 °C and, as can be seen in Fig. 8, at 450 °C the spectrum recovered its good characteristics.

Although the physical reasons for the "curing" process after the 1st cycle are presently unknown, they may be related to a possible improvement of the electrical contact between the diode and the metal case (resistance decrease), which is made with silver sintering, and to

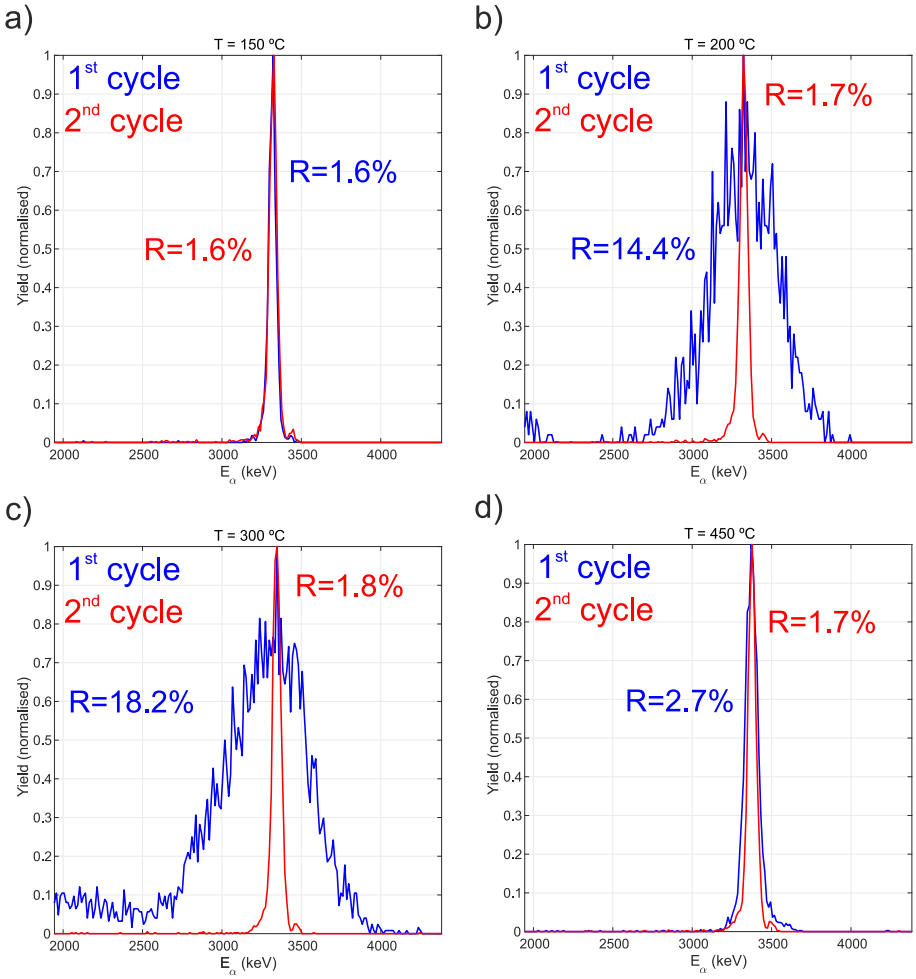

Fig. 8. Pulse height spectra recorded in the 1st heating and subsequent cooling cycle for temperatures ranging from 150 °C up to 450 °C.

the desorption of impurities. In the successive heating cycles the leakage current is much smaller (lower than 200 nA below 400 °C), as can be seen in Fig. 9.

The most remarkable result found in this work is that the energy resolution of the spectra in steady conditions (i.e. after the "curing" process) shows a good and fairly constant value of approximately 2% in the full temperature range (RT-450 °C), as shown in Fig. 10. This corresponds to a FWHM of ~54 keV. The FWHM has different contributions according to the following equation [Li et al., 2019]:

$$FWHM^2 = FWHM_s^2 + FWHM_o^2 + FWHM_N^2 \quad (1)$$

where $FWHM_s$ is associated with the statistics of electron-hole formation in the SiC material. $FWHM_o$ is related to the energy straggling of the ion beam in the entrance dead layers and $FWHM_N$ contains the contributions of the leakage current and the electronic noise. The calculations shown that $FWHM_s$ ~4.2 keV (assuming a Fano factor of ~0.13 for SiC [S.K. Chaudhuri et al., 2013]) and $FWHM_o$ ~15 keV (according to the SRIM simulations), so that the energy resolution is dominated by the term $FWHM_N$.

During the experimental measurements, it has been observed that the electronic noise exhibits behavior dependent on both the applied bias and the temperature. In the most unfavorable case, when the detector is reverse biased at 40 V and operated at a temperature of 450 °C, the overall noise appears around the 1 MeV region. Considering our experimental setup (cables, encapsulation, etc.) and considering the detector's layout, including dead layers and the depletion zone width at 40 V, simulations carried out with SRIM code have demonstrated that the minimum energy of the He beam to be detected in our setup is when the energy of the He ions exceeds ≈1.3 MeV.

From the experimental results, the best detector performance occurred in the 2nd cycle, when the oven was completely off. After successive thermal cycles (four heating cycles and one cooling cycle), when the heater was turned on and off repeatedly, the resolution slightly worsened. However, this change in resolution is not drastic, ranging at 450 °C between 1.6% for the 2nd cycle (cooling) to 2.8% for the 5th cycle (heating).

For SiC Schottky diodes measured at high temperature using a ^{241}Am alpha source (E_α = 5485 keV), the values found in the literature for the

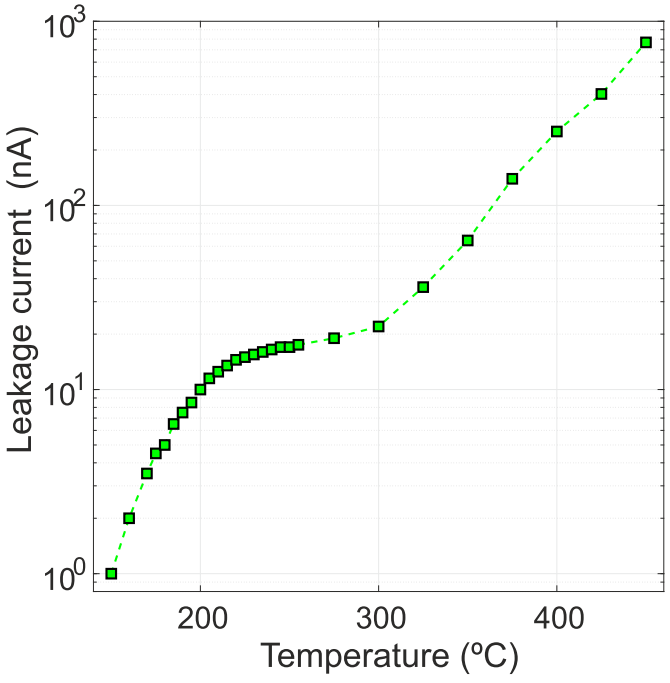

Fig. 9. Leakage current as a function of temperature.

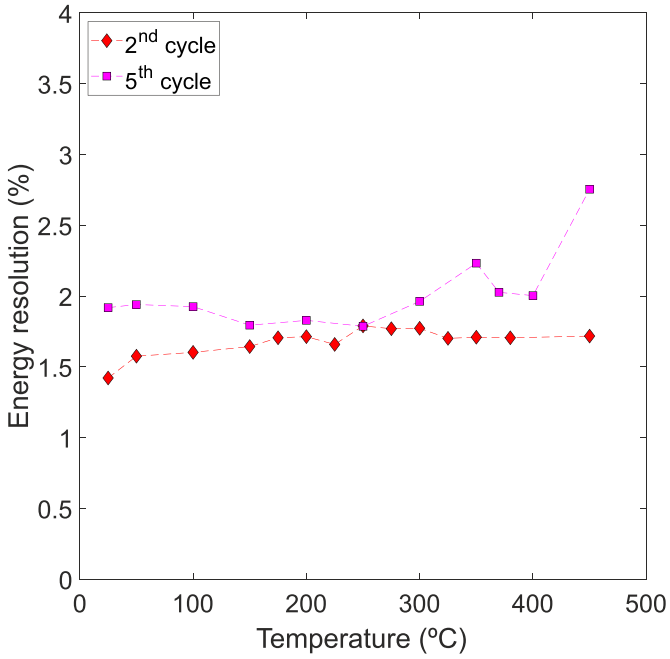

Fig. 10. Energy resolution as a function of temperature for the first and last cycles after the thermal annealing process. The detector maintained a consistently good energy resolution ($R \lesssim 2\%$).

energy resolution were 2.4% at 200 °C [Li et al., 2019] and between 2 and 3.5% at 500 °C [Jarrell, 2015]. Our results are comparable or slightly better, also considering that they were obtained using a 3.5 MeV He ion beam.

3.4. Average electron-hole pair creation energy as a function of temperature

In Fig. 11 different pulse height spectra obtained during the cooling cycle in the temperature range between 450 °C and RT are represented. Clearly, the peaks shift towards higher energies as the detector temperature rises.

Consistent with this result, the average energy for electron-hole pair creation, ϵ_{4H-SiC}, must decrease with increasing temperature. Accordingly, ϵ_{4H-SiC} was calculated from the energy shift in the spectra for the measured temperature range using equation (2),

$$\varepsilon_{4H-SiC}(T) = \varepsilon_{4H-SiC}(RT)\frac{E(RT)}{E(T)} \quad (2)$$

where E(T) and E (RT) are the measured energy values given by the centroid of the best-fit Gaussian at room temperature and applied temperature, respectively, and ϵ_{4H-SiC} (RT) is the average electron-hole pair creation energy at room temperature. The ϵ_{4H-SiC} value at RT was extracted from [Garcia et al., 2013], where similar measurements were carried out on a Schottky 4H–SiC detector. The associated uncertainty of the centroid was given by the statistic error of the best-fit Gaussian, while the experimental uncertainty of ϵ_{4H-SiC} was calculated from quadratic error propagation using eq. (2). This uncertainty is represented in Fig. 12 by the size of the experimental points. To analyze our experimental data, we applied the model introduced in [Garcia et al., 2013]:

$$\varepsilon_{4H-SiC} = E_g(T) - aT + b \quad (3)$$

Where E_g(T) represents the band gap of SiC as a function of temperature, which is modeled as follows:

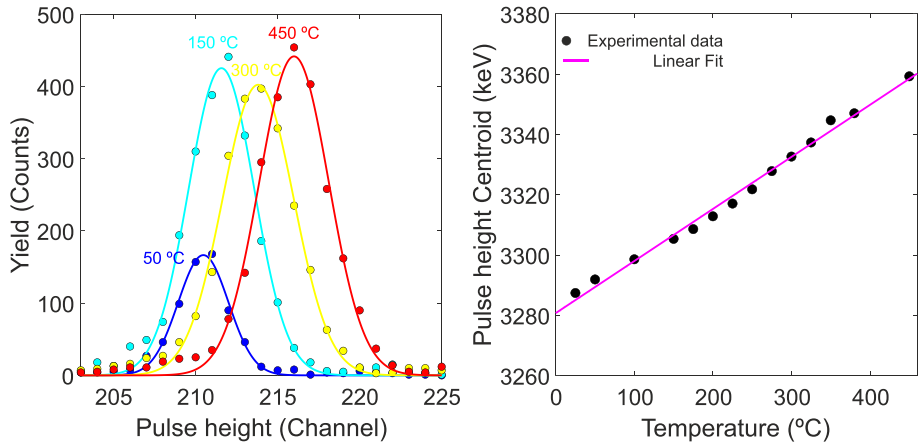

Fig. 11. Left-Pulse height spectra of 3.5 MeV alpha particles measured with the 4H–SiC PND detector at different temperatures between 50 °C and 450 °C. Right-shift of the centroid of the peaks toward higher energies indicating a decrease in electron-hole pair formation energy as temperature increases.

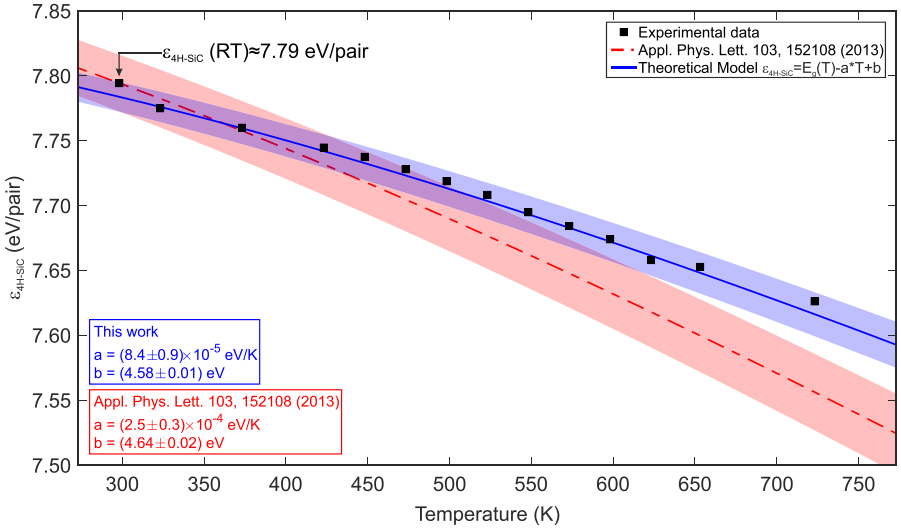

Fig. 12. Average electron-hole pair creation energy in 4H–SiC as a function of temperature. Experimental data from this work (black dots and blue line) and from [27] (red line) are shown.

$$E_g(T) = 3.265 - 6.5 \times 10^{-4} \frac{T^2}{T + 1300} \ (eV) \tag{4}$$

In the previous models, the temperature is given in K. The comparison between our experimental results with the data available in the literature [Garcia et al., 2013], are shown in Fig. 12.

The fitting coefficients obtained were a $= (8.4 \pm 0.9) \times 10^{-5}$ eV/K and b $= (4.58 \pm 0.01)$ eV/K. The shaded error bands represent the uncertainty in the determination of ϵ_{4H-SiC} associated with the coefficients of the models used for the analysis. Our experimental results present a good agreement with those available in [Garcia et al., 2013]. The difference in ϵ_{4H-SiC} values at 500 °C extracted from the fit curves is only 1%, which is our uncertainty in the ϵ_{4H-SiC} values.

While the trend of the ϵ_{4H-SiC} curves versus temperature are clearly distinctive, the differences may be due to several factors, including the fact that the comparison is for different kind of devices: a PN junction versus a Schottky diode. Regarding the testing implementation, current data were obtained with a monoenergetic 3.5 MeV alpha beam instead of a ^{241}Am radioactive source, which has three main alpha emissions at different energies, so the treatment of the peaks to obtain the centroid energy is intrinsically more complex and may entail additional uncertainties or parasitic effects. Nonetheless, the spectra obtained in [Garcia et al., 2013] at high temperature (450 °C) present a FWHM ~ 500 keV and very low statistics (see Figs. 2 and 4 in the above reference), which again may have introduced considerable error or certain distortion of the very curve trend.

4. Conclusions

In this work, the potential use of a new type of 4H–SiC detector designed to measure suprathermal ions in future nuclear fusion devices has been studied. For this purpose, the spectroscopic properties of a 4H–SiC PND have been tested and analyzed at different temperatures, ranging from RT to 450 °C by means of the IBIC technique and using a monoenergetic 3.5 MeV He^{2+} beam. It is clear from the energy resolution measurements that, during the 1st heating cycle, a beneficial annealing is produced and, after this "curing" process, the detector provides excellent energy resolution $\lesssim$2% in the full temperature range up to 450 °C for the detection of 3.5 MeV alpha particles. While the observed behavior cannot be considered entirely universal, it is highly recommended to incorporate a vacuum annealing process as a fundamental strategy in the working methodology before employing the detector. This approach significantly aids in mitigating the effects of outgassing and ensures the stabilization of the leakage current. The

experimental results obtained in our work significantly improve upon the measurements conducted by other authors for the energy resolution of SiC detectors at high temperature.

Additionally, the energy spectra obtained at different temperatures allowed us to obtain the value of the average electron-hole pair creation energy with better accuracy than in the previous works, which can be very important for a correct interpretation of the energy peaks measured at high temperatures. The overall results show the capability of this 4H–SiC PND for the detection of fast ions, including fusion-born alpha particles, escaping from the plasma as expected in the next generation of thermonuclear fusion reactors like ITER. Future work will investigate the radiation hardness of this type of detectors also at different temperatures to find the operating limits of the device.

Declaration of competing interest

The authors declare that they have no known competing financial interests or personal relationships that could have appeared to influence the work reported in this paper.

Data availability

The data that has been used is confidential.

Acknowledgements

This research was funded by the Spanish Ministry of Science, Innovation and Universities grant numbers RTC-2017-6369-3 (FEDER/EU) and ICTS-2020-02 US-4 (FEDER/EU), the Regional Ministry of Economy, Knowledge, Business and University grant number US-1380791, the Spanish Ministry of Science, Innovation grant number PID 2020 116822RB-I00 and PID 2021-124660OB-C22.

M.C. Jiménez-Ramos acknowledges the support to this work through a VI PPIT-US contract.

References

Alter Technology company, 2023. https://www.altertechnology-group.com/es/nuestra-empresa/alter-technology-espana/.

Aumeunier, M.H., Kočan, M., Reichle, R., Gauthier, E., 2017. Impact of reflections on the divertor and first wall temperature measurements from the ITER infrared imaging system. Nucl. Mater. Energy. 12, 1265–1269. https://doi.org/10.1016/j.nme.2017.02.014.

Breese, M.B.H., 1993. A theory of ion beam induced charge collection. J. Appl. Phys. 74, 3789. https://doi.org/10.1063/1.354471.

Cavallaro, S., Torrisi, L., Cutroneo, M., Krása, J., Ullschmied, J., 2014. Neutron fluences of the D-D fusion reaction at 1016 W/cm2 laser-target interactions. J. Phys. Conf. Ser. 508, 012023 https://doi.org/10.1088/1742-6596/508/1/012023.

Chaudhuri, S.K., Zavalla, K.J., Mandal, K.C., 2013. Experimental determination of electronhole pair creation energy in 4H-SiC epitaxial layer: an absolute calibration approach. Appl. Phys. Lett. 102 (3) https://doi.org/10.1063/1.4776703. #031109.

Crnjac, A., Skukan, N., Provatas, G., Rodriguez-Ramos, M., Pomorski, M., Jakšić, M., 2020. Electronic properties of a synthetic single-crystal diamond exposed to high temperature and high radiation. Materials 13, 2473. https://doi.org/10.3390/ma13112473.

Dankowski, J., Drozdowicz, K., Kurowski, A., Wiącek, U., Nowak, T., Zabila, Y., 2017. Diamond detectors for spectrometric measurements of fusion plasma products. Diam. Relat. Mater. 79, 88–92. https://doi.org/10.1016/j.diamond.2017.08.016.

Galdon-Quiroga, J., Garcia-Munoz, M., Sanchis-Sanchez, L., Mantsinen, M., Fietz, S., Igochine, V., Maraschek, M., Rodriguez-Ramos, M., Sieglin, B., Snicker, A., Tardini, G., Vezinet, D., Weiland, M., Eriksson, L.G., the ASDEX Upgrade Team., the EUROfusion MST1 Team, 2018. Velocity space resolved absolute measurement of fast ion losses induced by a tearing mode in the ASDEX Upgrade tokamak. Nucl. Fusion 58, 036005. https://doi.org/10.1088/1741-4326/aaa33b.

Garcia, T.R., Kumar, A., Reinke, B., Blue, E., T, Wind, W., 2013. Electron-hole pair generation in SiC high-temperature alpha particle detectors. Appl. Phys. Lett. 103, 15210 https://doi.org/10.1063/1.4824774.

García López, J., Ager, F.J., Barbadillo Rank, M., Madrigal, F.J., Ontalba, M.A., Respaldiza, M.A., Ynsa, M.D., 2000. CNA: the first accelerator-based IBA facility in Spain. Nucl. Instrum. Methods B 161–163, 1137–1142. https://doi.org/10.1016/S0168-583X(99)00702-8.

Garcia Lopez, J., Jimenez-Ramos, M.C., Rodriguez-Ramos, M., Ceballos, J., Linez, F., Raisanen, J., 2016. Comparative study by IBIC of Si and SiC diodes irradiated with high energy protons. Nucl. Instrum. Methods Phys. Res. B 372, 143–150. https://doi.org/10.1016/j.nimb.2015.12.029.

García-Muñoz, M., Fahrbach, H.U., Zohm, H., the ASDEX Upgrade Team, 2009. Scintillator based detector for fast-ion losses induced by magneto hydrodynamic instabilities in the ASDEX upgrade tokamak. Rev. Sci. Instrum. 80, 053503 https://doi.org/10.1063/1.3121543.

Garcia-Munoz, M., Kocan, M., Ayllon-Guerola, J., Bertalot, L., Bonnet, Y., Casal, N., Galdon, J., Garcia Lopez, J., Giacomin, T., Gonzalez-Martin, J., Gunn, J.P., Jimenez-Ramos, M.C., Kiptily, V., Pinches, S.D., Rodriguez-Ramos, M., Reichle, R., Rivero-Rodriguez, J.F., Sanchis-Sanchez, L., Snicker, A., Vayakis, G., Veshchev, E., Vorpahl, Ch, Walsh, M., Walton, R., 2016. Conceptual design of the ITER fast-ion loss detector. Rev. Sci. Instrum. 87, 11D829. https://doi.org/10.1063/1.4961295.

Gómez-Camacho, J., López, J.G., Guerrero, C., Gutiérrez, J.L., García-Tenorio, R., Santos-Arévalo, F.J., Chamizo, E., Ferrer, F.J., Jiménez-Ramos, M.C., Balcerzyk, M., Fernández, B., 2021. Research facilities and highlights at the centro nacional de Aceleradores (CNA). Eur. Phys. J. Plus. 136, 1–16. https://doi.org/10.1140/epjp/s13360-021-01253-x.

Instituto de Microelectrónica de Barcelona (IMB-CNM-CSIC), 2023. https://www.imb-cnm.csic.es/es.

Jarrell, Joshua T., 2015. High Temperature Characterization and Endurance Testing of Silicon Carbide Schottky Barrier Alpha Detectors. Master's Thesis. The Ohio State University.

Jiménez-Ramos, M.C., García López, J., García-Muñoz, M., Rodríguez-Ramos, M., Carmona Gázquez, M., Zurro, B., 2014. Characterization of scintillator materials for fast-ion loss detectors in nuclear fusión reactors. Nucl. Instrum. Methods B. 332, 216–219. https://doi.org/10.1016/j.nimb.2014.02.064.

Jiménez-Ramos, M.C., López, J.G., Osuna, A.G., Rodríguez-Ramos, M., Barroso, A.V., Muñoz, M.G., Andrade, E., Pellegrini, G., Otero Ugobono, S., Godignon, P., Rafi, J. M., Rius, G., 2020. IBIC analysis of SiC detectors developed for fusion applications. Radiat. Phys. Chem. 177, 109100 https://doi.org/10.1016/j.radphyschem.2020.109100.

Lebedev, A.A., Kozlovski, V.V., Davydovskaya, K.S., Levinshtein, M.E., 2021. Radiation hardness of silicon carbide upon high-temperature electron and proton irradiation. Materials 14, 4976. https://doi.org/10.3390/ma14174976.

Leroy, C., Rancoita, P.G., 2012. Silicon Solid State Devices and Radiation Detectors. Word Scientific, 978-981-4390-04-0.

Levinshtein, M.E., Rumyantsev, S.L., Shur, M.S. (Eds.), 2001. Properties of Advanced Semiconductor Materials: GaN, AIN, InN, BN, SiC, SiGe. John Wiley & Sons.

Li, Zheng, Wu, Jian, Wu, Kunlin, Fan, Yikui, Bai, Zhongxiong, Jiang, Yong, Yin, Yanpeng, Xie, Qilin, Lei, Jiarong, 2019. The performance of 4H–SiC detector at high temperature after gamma irradiation. Radiat. Phys. Chem. 162, 153–156. https://doi.org/10.1016/j.radphyschem.2019.05.004.

Medina, E., Sangregorio, E., Crnjac, A., Romano, F., Milluzzo, G., Vignati, A., Jakšic, M., Calcagno, L., Camarda, M., 2023. Radiation hardness study of silicon carbide sensors under high-temperature proton beam irradiations. Micromachines 14 (1), 166. https://doi.org/10.3390/mi14010166.

Nava, F., Castaldini, A., Cavallini, A., Errani, P., Cindro, V., 2006. Radiation detection Properties of 4H-SiC Schottky diodes irradiated up to 1016 n/cm2 by 1 MeV neutrons. IEEE Trans. Nucl. Sci. 53 (5), 2977–2982. https://doi.org/10.1109/TNS.2006.882777.

Nava, F., Bertuccio, G., Cavallini, A., Vittone, E., 2008a. Silicon carbide and its use as radiation detector material. Meas. Sci. Technol. 19, 102001. http://10.1088/0957-0233/19/10/102001.

Pezzarossa, M., Cepparrone, E., Cosic, D., Jakšić, M., Provatas, G., Vićentijević, M., Vittone, E., 2021. Polychromatic angle resolved IBIC analysis of silicon power diodes. Nucl. Instrum. Methods B. 488, 50–63. https://doi.org/10.1016/j.nimb.2020.12.006.

Ramos, M.R., Crnjac, A., Provatas, G., Grilj, V., Skukan, N., Pomorski, M., Jakšić, M., 2021. Characterization of ion beam induced polarization in scCVD diamond detectors using a microbeam probe. Nucl. Instrum. Methods B. 504, 21–32. https://doi.org/10.1016/j.nimb.2021.07.013.

Ramos, M.R., Crnjac, A., Cosic, D., Jakšić, M., 2022. Ion microprobe study of the polarization quenching techniques in single crystal diamond radiation detectors. Materials 15, 388. https://doi.org/10.3390/ma15010388.

Rivero-Rodriguez, J.F., Garcia-Munoz, M., Martin, R., Galdon-Quiroga, J., Ayllon-Guerola, J., Akers, R.J., Buchanan, J., Croft, D., Garcia-Vallejo, D., Gonzalez-Martin, J., Harvey, D., McClements, K.G., Rodriguez-Ramos, M., Sanchis, L., 2018. A rotary and reciprocating scintillator based fast-ion loss detector for the MAST-U tokamak. Rev. Sci. Instrum. 89, 10I112. https://doi.org/10.1063/1.5039311.

Rodríguez Ramos, M., 2017. Calibración absoluta y aplicación de los detectores de pérdidas de iones rápidos basados en materiales centelleadores para dispositivos de fusión nuclear. PhD. Universidad de Sevilla, Sevilla.

Rodriguez-Ramos, M., Garcia-Munoz, M., Jimenez-Ramos, M.C., Garcia Lopez, J., Galdon Quiroga, J., Sanchis-Sanchez, L., Ayllon-Guerola, J., Faitsch, M., Gonzalez-Martin, J., Hermann, A., Marne, P., Rivero-Rodriguez, J.F., Sieglin, B., Snicker, A., the ASDEX Upgrade Team, 2017. First absolute measurements of fast-ion losses in the ASDEX Upgrade tokamak. Plasma Phys. Contr. Fusion 59, 105009. https://doi.org/10.1088/1361-6587/aa7e5f.

Rodríguez-Ramos, M., Jiménez-Ramos, M.C., García-Muñoz, M., García López, J., 2017. Temperature response of several scintillator materials to light ions. Nucl. Instrum. Methods B. 403, 7–12. https://doi.org/10.1016/j.nimb.2017.04.084.

Simon, M., Sze, 2002. Semiconductor Devices: Physics and Technology, second ed. 0-471-33372-7.

Thyagaraja, A., Schwander, F., McClements, K.G., 2007. Rotation driven by fast ions in tokamak. Phys. Plasmas 14, 112504. https://doi.org/10.1063/1.2801716.

Torrisi, L., 2014. Ion acceleration and D-D nuclear fusion in laser-generated plasma from advanced deuterated polyethylene. Molecules 19, 17052–17065. https://doi.org/10.3390/molecules191017052.

Torrisi, L., Cannavò, A., 2016. Silicon carbide for realization of “telescope” ion detectors. IEEE Trans. Electron. Dev. 63, 4445–4451. https://doi.org/10.1109/TED.2016.2612237.

White, R.B., Fredrickson, E., Darrow, D., Zarnstorff, M., Wilson, R., Zweben, S., Hill, K., Chen, Y., FuWhite, R.G., 1995. Toroidal Alfvén eigenmode-induced ripple trapping. Phys. Plasmas 2, 2871. https://doi.org/10.1063/1.871452.

Ziegler, J.F., Biersack, J.P., Littmark, U., 2008. The Stopping and Range of Ions in Solids. Pergamon, New York. http://refhub.elsevier.com/S0969-806X(19)31518-X/sref25.